Optics and Laser Technology 115 (2019) 268–276

Contents lists available at ScienceDirect

Optics and Laser Technology

journal homepage: www.elsevier.com/locate/optlastec

Full length article

Effect of separate confinement hetero-structure layer on tunnel injection transistor laser-based transmitter for high-speed optical communication networks

Jaspinder Kaur[a,*], Rikmantra Basu[a], Ajay K Sharma[b]

[a] Department of Electronics and Communication Engineering, National Institute of Technology Delhi, Narela, Delhi 110040, India
[b] Department of Computer Science and Engineering, Dr. B. R. Ambedkar National Institute of Technology Jalandhar, Punjab 144011, India

HIGHLIGHTS

- Study and analysis is focused on use of Group III-V material.
- Discussion on structures, performances, and results related to some important works.
- Comparison of some important characteristics of TI-MQW-TL by varying SCH width.
- Proposed structure shows better performance than previously reported works.

ARTICLE INFO

Keywords:
Multiple quantum well
Heterojunction Bipolar Transistors
Threshold current
Transistor laser
Tunneling

ABSTRACT

Transistor Laser has already established as a promising candidate for high speed optical interconnects and optical telecommunication networks. The present work is focused on the performance of multiple quantum wells (MQW) based transistor laser by incorporating tunnel injection phenomenon and it's performance by varying the width of the separate confinement heterostructure layer. The virtual state (VS) is assumed as a path for the movement of injected charge carriers from bulk to nanostructures. We have estimated the various characteristics such as base threshold current, light power output, and optical modulation response by considering various physical parameters such as diffusion time, gain compression factor, optical confinement factor, photon lifetime, tunneling time and diffusion length, as a function of separate confinement hetero-structure (SCH) layer thickness. It is found that with increasing thickness of the SCH layer, base threshold current reduces, the light output power increases, but the optical modulation response remains almost constant, which ensures the potentiality of the proposed structure for high speed opto-electronic transmitter with low power consumption.

1. Introduction

Optical transmitters are the backbone networks for many applications such as fiber-to-the-home (FTTHs), high-speed data transmission, and interconnections between computers. Earlier laser diodes (LDs) used to meet all these requirements as they have low cost and power consumption. However, due to the damping effect, the modulation speed of LDs is limited up to 40 Gb/s. Now a day, transistor laser (TLs) is the potential candidate for high-speed optical data transmission and of replacing LDs. The active layer incorporates Quantum Well (QW) into the base of a Heterojunction Bipolar Transistor (HBT) reported by Holonyak et al. [1,2]. Under normal active mode of operation, when the excess charge carriers sufficiently injected into the base, population inversion takes place between the conduction and the valence subbands of the QW. The structure is enclosed in a resonant cavity to provide proper optical feedback leading to self-sustained oscillation [2–4]. Holonyak's group proved that the device structure with a fast base recombination lifetime (30 picoseconds) can generate an optical output at a high modulation rate (22 Gbps) with transmission less prone to errors.

Since its announcement, the group led by Holonyak reported in various publications [5–10] provide the characteristics and performance of TLs. Some experimental works have also been performed by other groups on room temperature continuous wave operation of TLs [11–14]. Analytical and numerical models for terminal currents, light power output and optical modulation response of TLs reported by some

* Corresponding author.
E-mail addresses: jaspinderkaur@nitdelhi.ac.in (J. Kaur), rikmantrabasu@nitdelhi.ac.in (R. Basu).

https://doi.org/10.1016/j.optlastec.2019.02.038
Received 28 September 2018; Received in revised form 21 December 2018; Accepted 12 February 2019

other groups [15–19]. Basu et al. [20–24] have developed complete analytical models for base threshold current, optical modulation response and light power output including resonance-free modulation response of TLs. In addition, by incorporating multiple QWs (MQWs) into the base there is a substantial decrease in base threshold current [24]. To enhance the optical modulation response, it is necessary to reduce the base recombination lifetime with the incorporation of multiple quantum wells and a quantum dot, as already established in earlier works [21,23–24].

In conventional TL structures, it is not easy to fulfill both the requirements of getting high optical modulation response and low base threshold current simultaneously [24]. However, improving the speed of TL into terahertz and beyond, becomes a challenging task to accommodate maximum number of users in the same channel. A very effective approach may be to introduce a tunnel injection (TI) phenomenon, as it has been established in the conventional QW lasers [25–26]. The charge carriers from the emitter terminal enter into the QW regions by using the tunneling phenomenon, thereby increasing the speed. This concept has been utilized by kumar et al. [27] to propose and study the TI - TL. The authors have taken different tunneling probability values i.e. 0 to 1 and found a significant improvement in the optical modulation response in the Tunnel-TL structure, as well as a substantial decrease in base threshold current, from the calculated values found in MQW TLs without tunnel injection phenomenon [24]. To improve the performance further, it is of interest to investigate the role of separate confinement heterostructure (SCH) layers on the performance of TI MQW TL. Variation of the thickness of SCH layers has a substantial effect on DC and AC characteristics of the structure. In the present work, we vary the thickness of SCH layers and comparison is made for base threshold current, light output power and optical modulation response with the previous results reported by Kumar et al. [27] for a fixed SCH thickness. We have found a substantial reduction in base threshold current; however, modulation bandwidth remains almost the same. We have also found that the maximum confinement factor achievable is almost 30% for an SCH layer width of 26 nm.

The objective of this work is to propose a design for high-speed transmitter, by introducing tunneling phenomena and its effect on the variation of width of SCH layers. The novelty lies in proposing a suitable design for practical fabrication, where, the separate confinement heterostructure (SCH) layer is found to have a significant influence on the carrier distribution in multiple quantum well structure. Further advantages include easier fabrication of surface grating-based lasers and ridge lasers, the reduction of growth time and source-material use, and the more effective removal of heat due to lower thermal resistance. The differential quantum efficiency may found to be more sensitive to SCH-layer thickness, as well.

The rest of the paper paper is organized as follows: The device structure and band diagram are given in Section 2. The theory to obtain terminal currents, optical characteristics and modulation bandwidth with relevant expressions are given in Section 3. Results and discussions are presented in Section 4, and in Section 5 conclusions are drawn.

2. Device structure and band diagram

The Schematic of the Tunnel injection MQW TL is shown in Fig. 1(a) where $In_{0.2}Ga_{0.8}As/GaAs$ n-p-n heterojunction bipolar transistor structure is used. InGaP (n-type) material acts as an emitter, GaAs (p-type) material acts as a base and the collector is of n-GaAs. The active layer for lasing action is made of three $In_{0.2}Ga_{0.8}As$ quantum wells (QWs) having width of 16 nm each and GaAs barriers width of 4 nm each inserted in the p-GaAs base. Two AlAs SCH layers (having variable widths 21, 24 and 26 nm for performance study) used as a protection wall between QWs and barriers to reduce the leakage current. The collector layer is lattice- matched with the n-type GaAs buffer layer which helps for the subsequent growth of wells and barriers and the cubic based multilayer system grow along (1 0 0) axis.

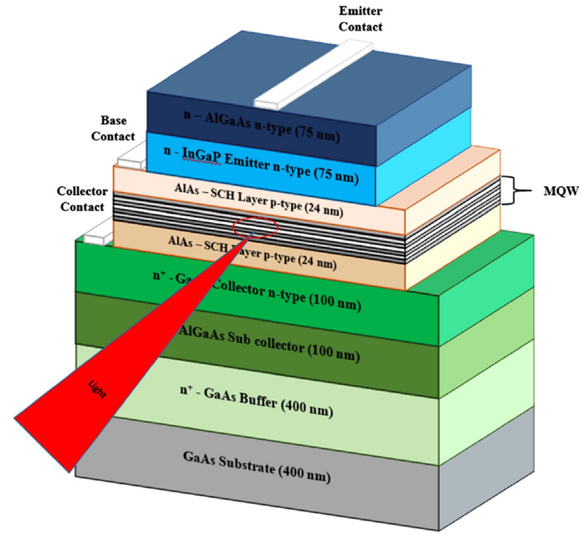

(a)

Fig. 1a. Schematic of the MQW tunnel injection transistor laser structure.

In the present work, the structure considered is almost identical with the structure proposed by Kumar et al. [27]. Since hot carriers are suppressed to be in the active region due to direct tunneling into low energy bound states, the carrier density in the active region can be assumed to be fully two-dimensional. This allows us to avoid the use of capture-escape model to dynamically obtaining the bound state density in the active region. One of the interesting features is that TL is expected to have a short radiative recombination lifetime as compared to the diode lasers (DLs).

The band diagram of the device structure has been simulated with the industrial standard (SILVACO-TCAD) software and is shown in Fig. 1b. The tunneling probability is represented by parameter f, whose, value lies between 0 and 1. The pure classical model is represented by f = 0; otherwise, it represents pure tunneling model [26]. The differential gain in the structure is calculated using Lorentzian broadening, 2D density-of-states, Fermi golden rule, and polarization dependent momentum matrix element [8]. In the calculation of terminal currents and rate equations, the tunneling carriers in 2D virtual states (VS) are involved [11]. Table 1 represents the structural parameters of the various device layers of the structure. Fig. 2 shows the SILVACO simulated band-to-band tunneling internally in the MQW regions.

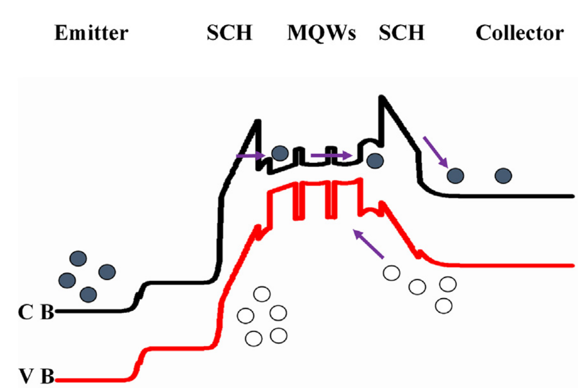

(b)

Fig. 1b. Band diagram of the MQW tunnel - transistor laser structure. Solid and empty balls represent electrons and holes, respectively.

Table 1
Parameters of various device layers of the structure.

Layer	Composition	Thickness (nm)	Doping (/cm^3)
Emitter	InGaP or AlGaAs	150	n-type 3×10^{20}
SCH Layer	AlAs	21, 24 and 26	p-type 1×10^{17}
Barrier	GaAs	4	p-type 4×10^{18}
QW	InGaAs	16	intrinsic
Collector	GaAs	100	n-type 2.2×10^{18}
Sub-collector	AlGaAs	100	n-type 2.2×10^{18}
Substrate	GaAs	400	–

3. Theory

The $In_{1-x}Ga_xAs$ QW layers are subjected to have compressive strain while inserting into the undoped GaAs base. The strain coefficients, $E_{C,str}$, $E_{V,str}$, and strain effect values, respectively, are described in [20]. In this analysis, only the first subbands of the conduction band (CB) and valence bands (VB) are participated in the optical transitions in narrow QWs [20]. The theory and calculated expressions of optical gain for strained quantum well structures with photon energy $\hbar\omega$ are inspired from Lysak et al. [28]. The rate equations for the carrier density in the SCH region (N_L), the 2D carriers in well (N_{qwi}), the 3D carriers (virtual state carrier density) above well i(N_{vsi}), and photon density (S) are calculated from previously developed models [24,26,27].

3.1. Terminal current

For transport of minority carriers, the time-independent continuity equation for diffusion-dominated transport in the base is given by [24],

$$\frac{d^2\delta n}{dx^2} = \frac{\delta n}{D_n\tau_B} = \frac{\delta n}{L_D^2} \tag{1}$$

where
δn = excess electron density, τ_B = base recombination time, and L_D. = Diffusion length

Carrier concentration before the nth QW located at a position $x_n$becomes [24],

$$\delta N_n^-(x) = \left[\frac{N_{VSn}e^{\frac{-x_{n-1}}{L_D}} - (J_{VS})_{n-1}e^{-\frac{x_{n1}}{L_D}}}{2cosh\left(\frac{x_n - x_{n-1}}{L_D}\right)}\right]e^{x/L_D} + \left[\frac{N_{VS1}e^{\frac{x_{n-1}}{L_D}} + (J_{VS})_{n-1}e^{\frac{x_{n-1}}{L_D}}}{2cosh(\frac{x_n - x_{n-1}}{L_D})}\right]e^{-x/L_D} \tag{2}$$

where, J_{VS} and N_{VS} represents the current density and the electron density, respectively, of the virtual energy state (VS) and the equivalent virtual state (VS) current density before any nth QW can be given by,

$$J_{VSn}^- = \frac{qD_n}{L_D}N_{VSn}\frac{\sinh(x_n - x_{n-1}/L_D)}{\cosh(x_n - x_{n-1}/L_D)} - \frac{J_{VS_{n-1}}}{\cosh\left(x_n - \frac{x_{n-1}}{L_D}\right)} \tag{3}$$

In the same way, carrier concentration and the equivalent virtual energy state (VS) current density after the nth QW can be given by [8],

$$\delta N_n^+(x) = \left[\frac{-N_{VSn}e^{-W_B/L_D}}{2\sinh\left(\frac{W_B - x_n}{L_D}\right)}\right]e^{x/L_D} + \left[\frac{N_{VSn}e^{W_B/L_D}}{2sinh\left(\frac{W_B - x_n}{L_D}\right)}\right]e^{-x/L_D} \tag{4}$$

$$J_{VSn}^+ = -\frac{qD_n}{L_D}N_{VSn}tanh\left(\frac{W_B - x_n}{L_D}\right) \tag{5}$$

Thus complete virtual energy state (VS) current density above nth QW at x = $x_n - J = J_{VSn}^- - J_{VSn}^+$

$$J_{VS_{n-1}} = J_{VSn}cosh\left(\frac{x_n - x_{n-1}}{L_D}\right) + \frac{qD_nN_{VSn}}{L_D}\times\left[sinh\left(\frac{x_n - x_{n-1}}{L_D}\right) + \coth\left(\frac{W_B - x_n}{L_D}\right)cosh\left(\frac{x_n - x_{n-1}}{L_D}\right)\right] \tag{6}$$

3.1.1. Evaluation of emitter current

The emitter current expression for nth QWs in an MQW structure can be described as [8],

$$J_E = \frac{qD_n}{L_D}\left[\sum_{i=1}^{n}\left\{(N_{VS})_i\left[tanh\left(\frac{x_i - x_{i-1}}{L_D}\right) - coth\left(\frac{x_i - x_{i-1}}{L_D}\right)\right] + \frac{(N_{VS})_{i+1}}{sinh\left(\frac{x_n - x_{i-1}}{L_D}\right)} - \frac{(J_{VS})_i.\, L_D}{q.\, D_n}\right\} \times \prod_{m=1}^{i} cosh\left(\frac{x_m - x_{m-1}}{L_D}\right)\right] \tag{7}$$

Threshold emitter current expression becomes,

$$J_{E_{th}}(i) = \sum_{i=0}^{n}\frac{(q + D_n + N_{VS1})}{L_D}.\,[J_{E1}(i) + J_{E2}(i)] - \frac{(q + D_n + N_{VS3})}{L_D}.\,J_{E3(i)} \tag{8}$$

The conventional rule for base current is given by $J_B = J_E - J_C$ and equivalent, terminal currents can be determined for different positions across the base.

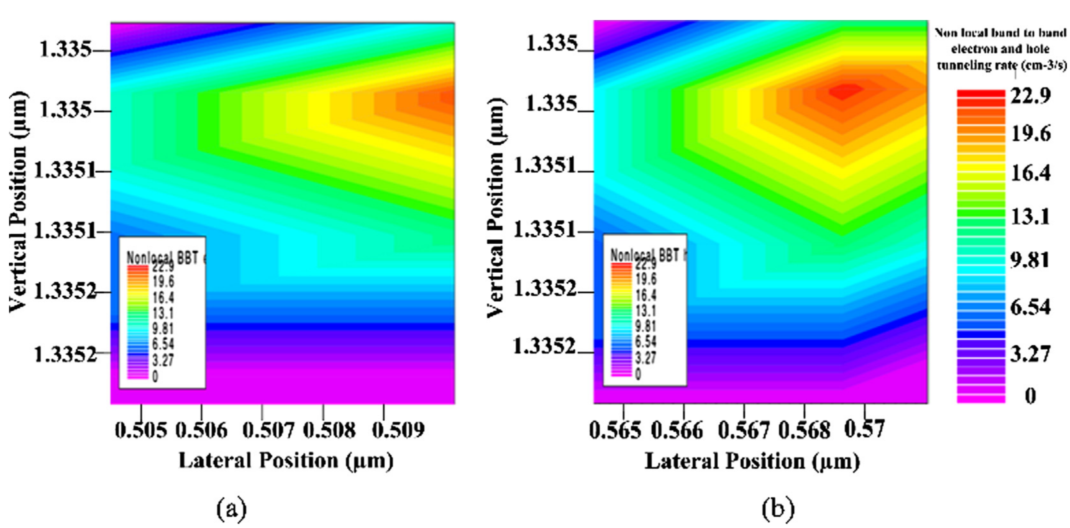

Fig. 2. Non- local band to band tunneling rate (a) electron tunneling rate (b) hole tunneling rate.

3.1.2. Collector current

Similarly, the collector current is estimated as [24],

$$J_C = \sum_{i=1}^{n}\left[\frac{J_E qD_n cosh\left(\frac{W_B - x_i}{L_D}\right)}{L_D cosh\left(\frac{x_i}{L_D}\right)cosh\left(\frac{x_{i+1}-x_i}{L_D}\right)}\right] - \sum_{i=1}^{n}\left[\frac{N_{VSi}qD_n \cosh\left(\frac{W_B - x_{i+1}}{L_D}\right)}{L_D cosh\left(\frac{x_{i+1}-x_i}{L_D}\right)}.\left\{coth\left(\frac{x_{i+1}-x_i}{L_D}\right)+\tanh\left(\frac{x_i}{L_D}\right)\right\}\right] - \sum_{i=1}^{n}\left[\frac{N_{VS_{i+1}}qD_n}{L_D}.\left\{\frac{cosh\left(\frac{W_B - x_{i+1}}{L_D}\right)}{sinh\left(\frac{x_{i+1}-x_i}{L_D}\right).\ cosh\left(\frac{x_{i+1}-x_i}{L_D}\right)} - sinh\left(\frac{W_B - x_{i+1}}{L_D}\right) + tanh\left(\frac{x_{i+1}-x_i}{L_D}\right)cosh\left(\frac{W_B - x_{i+1}}{L_D}\right)\right\}\right] + \sum_{i=1}^{n} J_{VS_{i+1}} cosh\left(\frac{W_B - x_{i+1}}{L_D}\right) \tag{9}$$

Threshold collector current density is given as,

$$J_{C_{th}}(i) = \sum_{i=0}^{n}\frac{(q.\ D_n.\ N_{VS3})}{L_D}.\ \sinh\left[\frac{W_B - x_{QW}(i)}{L_D}\right] \tag{10}$$

The carrier and current densities, respectively, related to the quantum well (QW) and the virtual energy states (VS) are estimated as [20],

$$\frac{J_{VS}}{qd} = \frac{J_{QW}}{qd} - \frac{N_{VS}}{\tau_S} \text{and} \ \frac{J_{VS}}{qd} = \frac{N_{VS}}{\tau_{cap}} - \frac{N_{QW}}{\tau_{esc}} \tag{11}$$

where, $\tau_{s,}$ τ_{cap} and τ_{esc} denote the spontaneous recombination lifetime, electron capture time into the quantum well (QW) and electron escape time from the quantum well (QW) to the virtual energy states (VS) respectively. The recombination current is larger than the laser current below lasing threshold ($J_B < J_{Bth}$). As, no stimulated emission takes place in the QW, so above the lasing threshold, population inversion occurs thereby considerably achieving the laser current much larger than the recombination current.

3.2. Statz De Mars laser rate equations

The Statz De Mars laser rate equations are used to estimate the optical characteristics of TL. where (S) denotes the photon density, (N_L) is SCH region carrier density. (N_{qwi}) and (N_{vsi}) denote, respectively, the 2-dimensional carrier densities in the well, and 3-dimensional carrier densities above the well for the i_{th} quantum well (QW) (i = 1, 2, 3) respectively [24]. Rest of the symbols have their usual meaning as in [24,27].

$$\frac{dN_L}{dt} = \frac{J}{q.\ L_{SCH}} - f\frac{N_L}{\tau_t} - (1-f)\frac{N_L}{\tau_d} \tag{12}$$

$$\frac{dN_{VS1}}{dt} = (1-f)\frac{N_L .L_{SCH}}{\tau_d.\ L_W} - N_{VS3}.\left(\frac{1}{\tau_d}+\frac{1}{\tau_c}+\frac{1}{\tau_n}\right) + \frac{N_{VS2}}{\tau} + \frac{N_{QW1}}{\tau} \tag{13}$$

$$\frac{dN_{QW1}}{dt} = f\frac{N.\ L_{SCH}}{\tau_d.\ L_W} - N_{QW1}.\left(\frac{1}{\tau}+\frac{1}{\tau_e}+\frac{1}{\tau_n}\right) + \frac{N_{VS1}}{\tau_C} + \frac{N_{QW2}}{\tau_t} + \frac{G.\ N_{QW1}.\ S}{1+\varepsilon.\ S} \tag{14}$$

$$\frac{dN_{VS2}}{dt} = -N_{VS1}.\left(\frac{2}{\tau_d}+\frac{1}{\tau_C}+\frac{1}{\tau_n}\right) + \frac{N_{VS3}+N_{VS2}}{\tau_d} + \frac{N_{QW2}}{\tau_S} \tag{15}$$

$$\frac{dN_{QW2}}{dt} = N_{QW2}.\left(\frac{2}{\tau_t}+\frac{1}{\tau_e}+\frac{1}{\tau_n}\right) + \frac{N_{VS2}}{\tau_C} + \frac{N_{QW3}-N_{QW1}}{\tau_t} - \frac{G.\ N_{QW2}.\ S}{1+\varepsilon S} \tag{16}$$

$$\frac{dN_{VS3}}{dt} = -N_{VS3}.\left(\frac{2}{\tau_d}+\frac{1}{\tau_C}+\frac{1}{\tau_n}\right) + \frac{N_{VS2}}{\tau_C} + \frac{N_{QW3}}{\tau_S} \tag{17}$$

$$\frac{dN_{QW3}}{dt} = -N_{QW3}.\left(\frac{1}{\tau_t}+\frac{1}{\tau_e}+\frac{1}{\tau_n}\right) + \frac{N_{VS3}}{\tau_C} + \frac{N_{QW2}}{\tau_t} + \frac{G.\ N_{QW3}.\ S}{1+\varepsilon.\ S} \tag{18}$$

and

$$\frac{dS}{dt} = \frac{G.\ S}{1+\varepsilon.\ S}\sum_{i=0}^{n}\Gamma_i.\ G.\ N_i - \frac{S}{\tau_P} \tag{19}$$

After performing AC and DC analysis, the modulation bandwidth is given as [23],

$$H_m(\omega) = \frac{S(\omega)}{S(0)} = \left[1 + 2j\frac{\omega.\ \Gamma_r}{\omega_r^2} - \left(\frac{\omega}{\omega_r}\right)^2\right] \tag{20}$$

The frequency of response is given by,

$$\omega_r = \sqrt{\frac{\left[\frac{f}{\tau_t} + \frac{(1-f)}{\tau_d}\right]}{\tau_P}} \tag{21}$$

where, τ_t and τ_d denotes the tunneling time and diffusion time constants, respectively. J is the current injection density, q is the charge of electron, τ_n is the recombination time of carriers. Let us suppose, carrier recombination does not take place in the SCH region. Then, τ_e and τ_C are the escape time from the QW state to the virtual energy states (VS) and capture time from the virtual energy state (VS) to the QW state respectively. L_W denotes the quantum well width (assumed to be equal), τ_P is the lifetime of photon, G is the optical gain, Γ is optical confinement factor and ε is the non-linear gain compression factor.

Upon solving Eqs. (12)–(19), the steady–state solutions are obtained by assuming steady state of operation The small-signal solution to these equations is achieved with the standard method of expressing the total quantities as (DC and AC) components as expressed, $X = X_0 + x(\omega).\ e^{i\omega t}$, $X = J,\ N_L,\ N_{QWi},\ N_{VSi}$, S; and $x(\omega) = j(\omega),\ n_L(\omega)$, $n_{QWi}(\omega)$, $n_{VSi}(\omega)$, $s(\omega)$.

4. Results and Discussion

The operation of the structure is considered at temperature 288 K. The parameters like permittivity, effective mass etc. are calculated by linear interpolation from the data available in the literature [20]. The values of the time constants are calculated from the literature [20]. The subband energies are based on finite barrier heights between well and barrier. The approximation method is used to calculate the subband energies and band offsets as given in [21–22,26]. Other parameters

Table 2
Values of parameters used in the calculations.

Absorption Coefficient, α	500 m^{-1}	Capture Time, $\tau_{capture}$	1 ps
Base Width, W_B	100 nm	Efficiency, η	0.8
SCH width	21,24 and 26 nm	Tunneling Time, τ_{tunnel}	0.094 ps
Reflectivity, R_1, R_2	0.32	Base Recombination Life Time, τ_B	200 ps

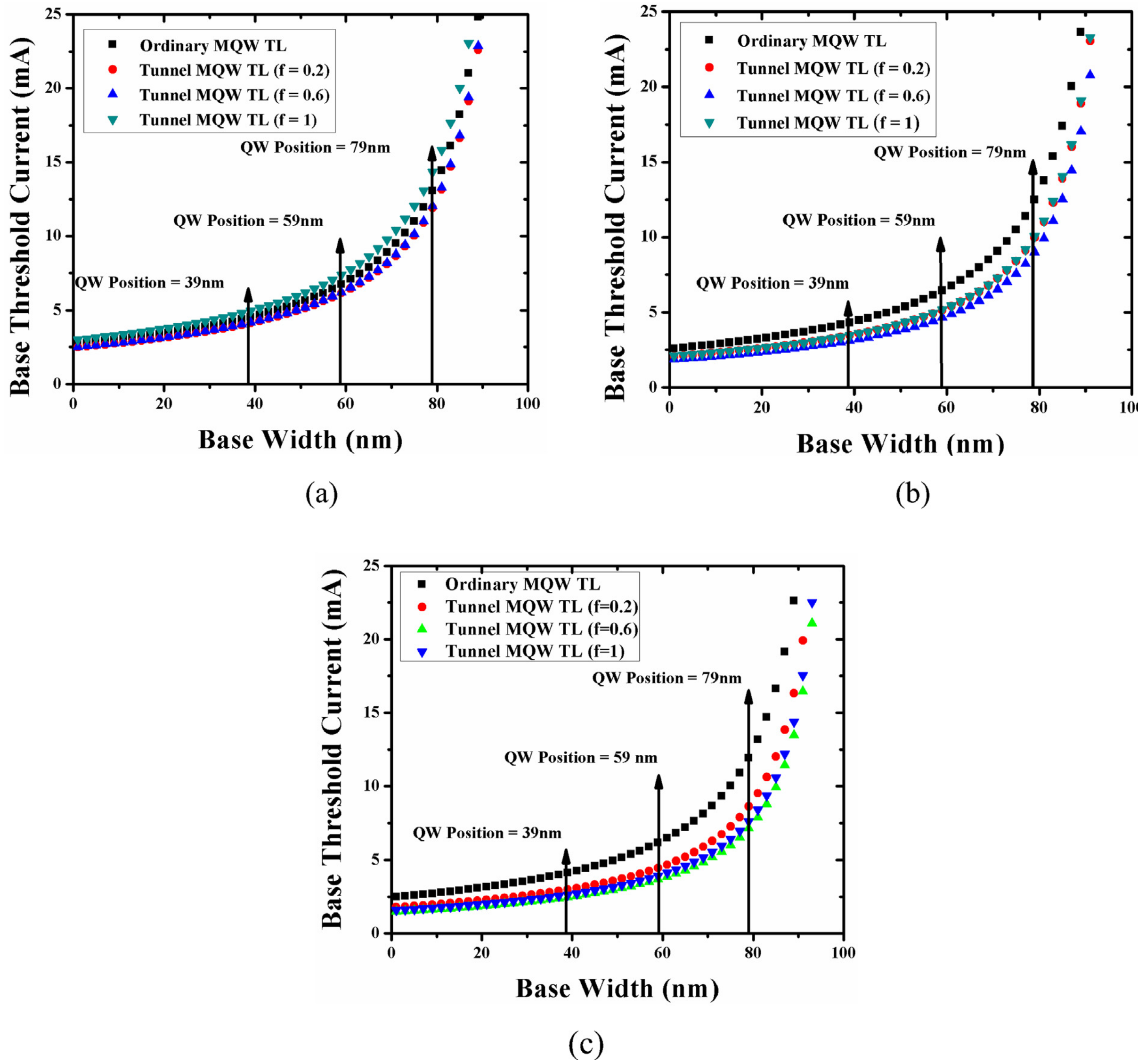

Fig. 3. Variation of base threshold current with base width for different QW positions for SCH layers (a) 21 nm, (b) 24 nm, and (c) 26 nm, respectively.

Table 3
Comparative study of the effect of SCH layer width variation on threshold base current.

SCH Layer width	Base Threshold Current I_{bth}(mA) QW Position (39 nm)			QW Position (59 nm)			QW Position (79 nm)		
	f = 0	f = 0.6	f = 1	f = 0	f = 0.6	f = 1	f = 0	f = 0.6	f = 1
21 nm	4.526	4.168	4.94	6.74	6.207	7.37	13.08	12.05	14.33
24 nm	4.317	3.112	3.47	6.429	4.63	5.17	12.46	8.984	10.05
26 nm	4.132	2.47	2.63	6.155	3.679	3.917	11.93	7.119	7.57

used in the calculations are described in Table 2 [24].

The alloy parameters such as bandgap, effective mass, permittivity, the density of states (NV 300 and NC 300) etc. are calculated using linear interpolation of the data [27]. At first QW position, initial virtual state carrier density is given as input (quite higher than transparency). In continuation, remaining QWs virtual state carrier density is calculated by the QW geometry factor that contributes the fraction of base charge captured in QW as, $\gamma_1 = (d/W_B)\left(1 - \frac{x_{QW1}}{W_B}\right)$. Thus, QW2 virtual state (VS) carrier density is estimated as, $N_{VS2} = N_{VS1}(1 - \gamma_1)$. Similarly, QW3 virtual state (VS) carrier density, $N_{VS3} = N_{VS2}(1 - \gamma_2)$ is calculated. Here, x_{QWi} are the locations of the ith position of the QW.

4.1. Effect of SCH width on base threshold current

Fig. 3 provides the variation of base threshold current with increasing base width of this structure for three different SCH layer thicknesses (21, 24, and 26 nm respectively), with different tunneling probability and with different quantum well positions at (39, 59, and 79 nm) as well, in the GaAs base of width 100 nm. These three configurations help to choose minimum base threshold current in terms of QW positions and of SCH thickness. The rate of rising in base threshold current increases as the QW position approaches towards the base-collector junction and base threshold current is lowest in case of symmetric MQW structures. It has been observed that at tunneling probability of 0.6, the lowest threshold base current may be achieved in this

Table 4
Comparative study of the effect of performance of threshold base current with existing results.

	SCH Layer width	Base Threshold Current I_{bth}(mA)								
		QW Position (39 nm)			QW Position (59 nm)			QW Position (79 nm)		
		f = 0	f = 0.6	f = 1	f = 0	f = 0.6	f = 1	f = 0	f = 0.6	f = 1
Single QW										
Ref. [20]	Without SCH Layer	–	–	–	21.5	–	–	–	–	–
Multiple QW										
Ref. [23,24]	Without SCH Layer	4.7598	–	–	7.06	–	–	13.7546	–	–
Ref. [27]	24 nm	4.76	2.91	2.99	7.08	4.32	4.45	13.75	8.38	8.62
Present work	21 nm	4.526	4.168	4.94	6.74	6.207	7.37	13.08	12.05	14.33
	24 nm	4.317	3.112	3.47	6.429	4.63	5.17	12.46	8.984	10.05
	26 nm	4.132	2.47	2.63	6.155	3.679	3.917	11.93	7.119	7.57

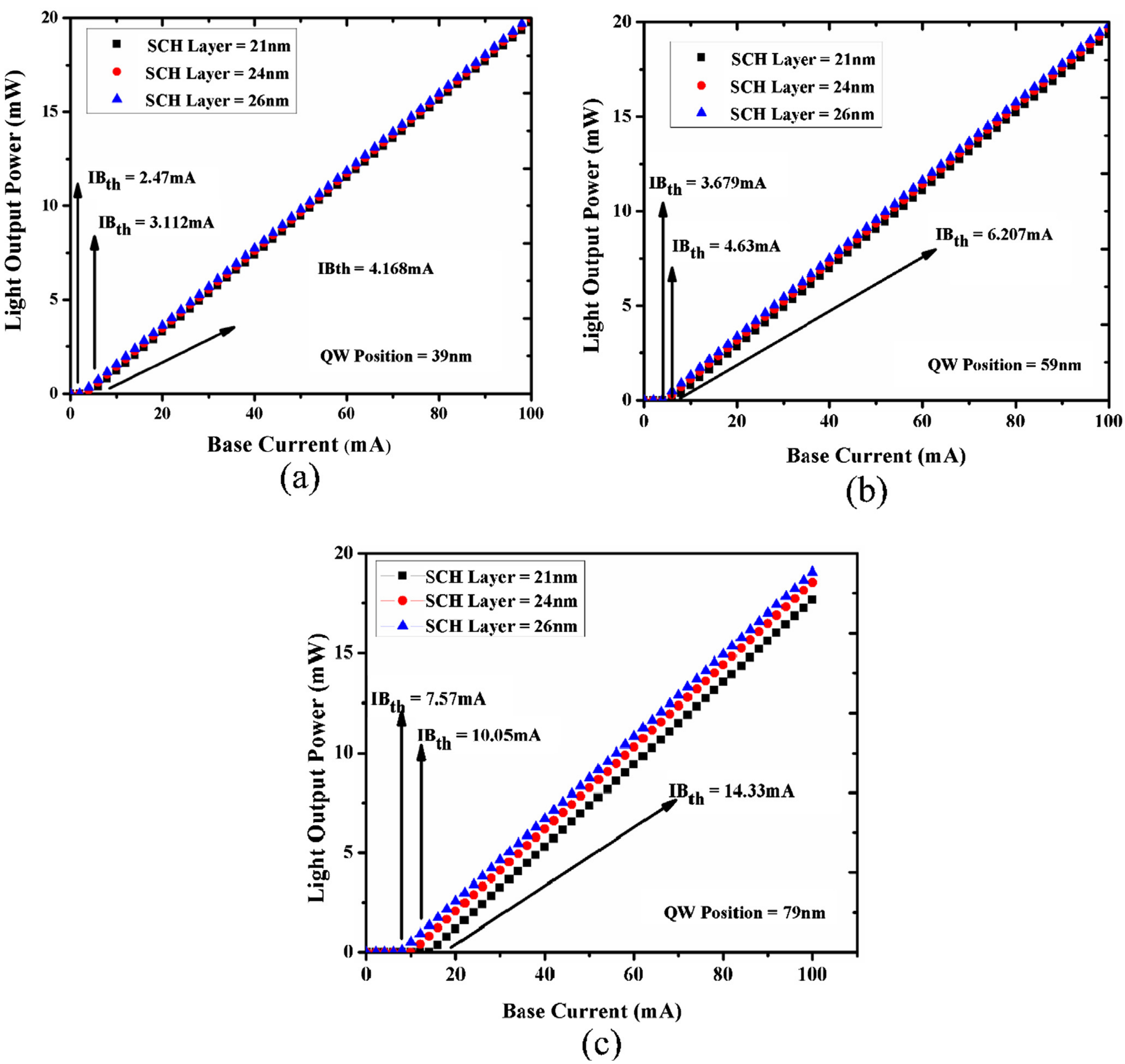

Fig. 4. Light output power as a function of base current for SCH Layers = (21 nm, 24 nm, 26 nm) at different QW positions (39, 59, and 79 nm) across the base.

Table 5
Comparative study of the effect of variation of SCH width on light output power.

Parameter	QW Position (nm)	SCH Layer = 21 nm (f = 0.6)	SCH Layer = 24 nm (f = 0.6)	SCH Layer = 24 nm (f = 0.6)	SCH Layer = 26 nm (f = 0.6)
		Present work	Present work	Ref. [27]	Present work
Base threshold current (I_{bth}), mA	39 nm	4.168	3.112	2.91	2.47
	59 nm	6.207	4.63	4.32	3.679
	79 nm	12.05	8.984	8.38	7.119

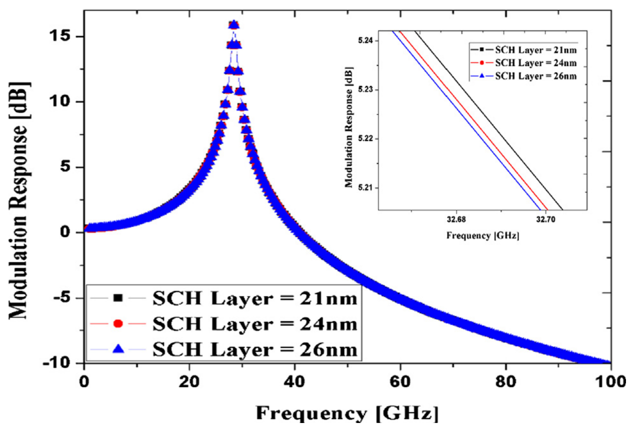

Fig. 5. Small-signal modulation response for different width of SCH layers.

proposed structure. The minimum value of the base threshold current is achieved with SCH width of 26 nm with tunneling probability of 0.6. This would be helpful in calculating light output power and other characteristics of MQW-TI-TL and to propose a optimum design of a proposed structure for practical fabrication. More importantly, closer the QW to the emitter-base junction, lower the base threshold current value in most of the device structures. As the QW position approaches the base-collector junction, sharper the base threshold current becomes.

Table 3 summarizes the conclusions drawn from Fig. 3, which clearly points out that minimum base threshold current is achieved with tunneling probability 0.6 with SCH layer width of 26 nm at different quantum well positions.

Table 4 compares the base threshold current performance of the proposed structure in the current literature with the existing results [20,23,24,27] for a validation of the proposed model. It clearly shows the various threshold base current for single and multiple quantum well transistor laser with and without the inclusion of SCH layer and tunnel injection phenomenon. As the basis of comparison, we have taken 21.5 mA for base threshold current of single QW positioned at 59 nm in the GaAs base [20], in which neither SCH layer nor tunneling probability is taken into account. For an MQW-TL structure, the calculated threshold base current is 7.06 mA obtained in the middle QW positioned at 59 nm without the inclusion of SCH layer and tunneling effect [23,24]. In addition, with the inclusion of SCH layer = 24 nm and tunnel injection mechanism in the MQW-TL structure [27], there is a substantial reduction in the base threshold current as illustrated in the table. Furthermore, if we increase the SCH layer width from 24 nm to 26 nm, the base threshold current starts decreasing and optimum results is obtained at probability 0.6. At low injected current level, there may not be much improvement in the base threshold current of the proposed

Table 7
Comparative study of the effect of variation of SCH width on modulation response with the existing results.

	Parameters	I_{bth} at (59 nm)/ Modulation Bandwidth		
Ref. [23]	Without SCH Layer	–	7.06 mA	–
	(f = 0)	–	25 GHz	–
Ref. [27]	With SCH	–	4.327 mA	–
	Layer = 24 nm	–	47.20 GHz	–
	(f = 0.6)			
Present work	With SCH Layer	6.207 mA	4.1 mA	3.6 mA
	(f = 0.6)	(21 nm)	(24 nm)	(26 nm)
		48.87 GHz	47.81 GHz	47.28 GHz

structure with SCH layer width 26 nm over 24 nm tunnel injection –TL one but the results may be significant at higher current injection level. These outcomes advocate of potential applications for this tunnel-injection transistor laser based transmitter to work at high speed optical communication networks.

4.2. Effect of SCH width on light output power

The estimated values of light output power with increasing base current for MQW-TI-TL for three SCH widths of 21 nm, 24 nm, and 26 nm respectively is shown in Fig. 4. The linear relationship between the calculated light output power and the base current is shown in the below equation [20],

$$P = \frac{(h\omega)}{q}\left[\frac{\alpha_m}{\alpha_m + \alpha}\right][I_b - I_{bth}] \tag{22}$$

where, α_m denotes the mirror loss and α represents the loss in the active layer. In this work, we also have considered three cases of QW positions at (39, 59, and 79 nm) with tunneling probability of 0.6 to compare the variation of light output power.

Table 5 represents a comparative study of the effect of the thickness of the SCH layer on light output power with the existing results. Here, we made comparison of laser light power for SCH layer width of 21 nm, 24 nm and 26 nm respectively. In case of 26 nm SCH layer width, base threshold current for the QW positioned at 39 nm (f = 0.6), 59 nm (f = 0.6) and 79 nm (f = 0.6) in the GaAs base of width 100 nm are 2.47 mA, 3.679 mA and 7.119 mA respectively. It appears that there is a decrease in base threshold current in 26 nm SCH layer width as compared to 24 nm SCH layer TL structure [27]. As, it is evident from the table that the reduction in the base threshold current is maximum in the SCH layer width of 26 nm and, at the same time, the rate of rise of laser light power is also maximum in this case.

Table 6
Comparative study of the effect of variation of SCH width on modulation response.

Parameters	SCH Layer = 21 nm (f = 0.6)	SCH Layer = 24 nm (f = 0.6)	SCH Layer = 26 nm (f = 0.6)
The base threshold current at 59 nm	6.207 mA	4.1 mA	3.6 mA
Modulation Bandwidth	48.87 GHz	47.81 GHz	47.28 GHz

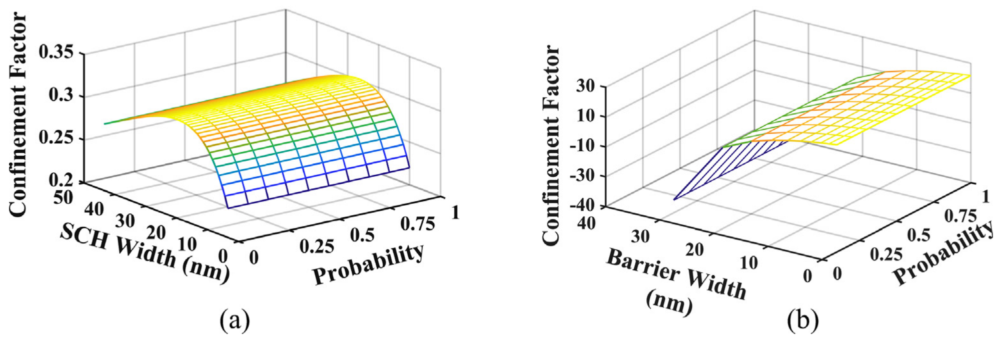

Fig. 6. Confinement factor as a function of increasing (a) SCH width (b) Barrier width of Tunnel-TL.

4.3. Effect of SCH width on modulation response

At a specific bias current, the modulation response H_m is described as the ratio of modulated photon number $S(\omega)$ to the corresponding unmodulated value $S(0)$ at a given frequency $\omega_m = 2\pi f_m$. The modulation Bandwidth, i.e. the 3-dB (3-decibel) frequency is expressed as the value of frequency at which the response falls to one-half of its value, and it is given as [23],

$$f_{3dB} = \frac{1}{2\pi}\sqrt{(f_r^2 - 2\Gamma_r^2) + 2\sqrt{(f_r^2 - 2\Gamma_r^2)^2 + f_r^2\Gamma_r^2}} \tag{23}$$

where the damping factor $\Gamma_r = \tau^{-1}$, and the effective lifetime τ is defined as,

$$\tau^{-1} = \tau_B^{-1} + \Gamma v_g gNS \tag{24}$$

In the above equation, the first term τ_B and the second term $\Gamma v_g gNS$, respectively, specify the base recombination lifetime and stimulated recombination lifetime. Photon density, $S = \eta(I_B - I_{Bth})/(q.\ v_g.\ \alpha_m)$ describes the ratio of number of photons per unit area. Here, group velocity (v_g), mirror loss (α_m), internal quantum efficiency (η) and usual base drive (I_B) responsible for stimulated emission from the QWs are considered from [23].

Fig. 5 depicts the effect of various SCH widths on modulation response with increasing frequency. It reveals that the modulation bandwidth remains almost constant with the variations of SCH width. Since increase or decrease of SCH width does not much affect the total number of carriers in the active region to alter the rate of recombination and it also does not depend upon the number of modulated photons, hence, the modulation bandwidth remains almost constant.

Table 6 enlists the comparative study of the effect of SCH width variation on modulation response. It may be concluded that the maximum bandwidth obtainable is 47.81 GHz, irrespective of SCH thickness.

Table 7 shows the performance of modulation bandwidth with the results available in existing literatures [24,27]. It depicts that, we have calculated the small signal modulation response and made a comparison of 3-dB modulation bandwidth, with and without the inclusion of SCH layer and tunnel injection mechanism in the MQW-TL device. As the basis of comparison, we have used 25 GHz modulation bandwidth of multiple QW positioned at 59 nm in the GaAs base of TL [23], in which SCH layer as well as tunneling probability is not taken into consideration. Additionally, when we consider SCH layer and tunneling effect into the structure then 47.20 GHz modulation bandwidth is obtained with tunneling probability f = 0.6 and SCH layer width is equal to 24 nm [27]. Furthermore, in the present work, we consider three cases of the SCH layer (21 nm, 24 nm and 26 nm) with tunneling probability 0.6. However, the modulation bandwidth remains almost constant with the variation of SCH layer width in the structure as shown in the table. Lastly, if we further increases the SCH layer thickness then modulation bandwidth will start decreasing. Hence, we deduced that SCH thickness = 26 nm is the optimum value to obtain the maximum modulation bandwidth at tunneling probability f = 0.6.

4.4. Effect of SCH width and barrier width on confinement factor

Fig. 6(a) and (b) show the confinement factor as a function of increasing SCH width and barrier width of Tunnel-TL respectively, which is more helpful in getting the best possible value of the confinement factor of Tunnel -TL. Fig. 6(a) undoubtedly indicates that the best possible value of 30% for confinement factor is achievable when SCH width increases from 24 nm to 26 nm, which is inconsistent with the analytical results obtained in our previous work by Kumar et al. [27]. Fig. 6(b) shows the confinement factor as a function of increasing barrier width and it depicts that the confinement factor decreases with increase of barrier width. It is evident that a maximum number of carriers will recombine at the barrier and will generate non-coherent light before going to the QW regions. Therefore, it can be deduced that the carrier and optical confinement, both the factors get reduced.

5. Conclusion

In this present work, the effect of variation of SCH width on base threshold current, light power output and optical modulation response of a tunnel injection TL structure having three QWs have been studied. An optimum value of 26 nm SCH width and a tunneling probability of 0.6 have been found to yield lowest base threshold current and high laser light power. However, the optical modulation response has not increased that significantly and the maximum value of 47.8 GHz has been obtained in the proposed structure. Thereby, it is expected that the present work will encourage researchers to increase the modulation bandwidth for optical communication and broadband networks to a higher value.

Acknowledgements

Jaspinder Kaur would like to thank MHRD (India), for providing financial support in the form of Junior Research Fellowship (JRF). All of the authors are thankful to Professor Praveen Kumar, Director, NIT Delhi, for his encouragement and support to undertake this work.

Appendix A. Supplementary material

Supplementary data to this article can be found online at https://doi.org/10.1016/j.optlastec.2019.02.038.

References

[1] G. Walter, N. Holonyak Jr., M. Feng, R. Chan, Laser operation of a heterojunction bipolar light-emitting transistor, Appl. Phys. Lett. 85 (2004) pp. 4768 (1-3).
[2] N. Holonyak Jr., M. Feng, The transistor laser, IEEE Spectrum 43 (2) (2006) 50–55.
[3] Han Wui Then, Milton Feng, Nick Holonyak Jr, "The transistor laser: theory and experiment", Proc IEEE 101 (2013) 2271–2298.
[4] P.K. Basu, Bratati Mukhopadhyay, Rikmantra Basu, Semiconductor Laser Theory,

CRC Press (T&F), Boca, Raton, USA, 2015 Ch 15.
[5] M. Feng, N. Holonyak Jr., A. James, K. Cimino, G. Walter, R. Chan, “Carrier lifetime and modulation bandwidth of a quantum well AlGaAs/ InGaP/ GaAs/ InGaAs transistor laser”, Appl. Phys. Lett. 89 (2006) pp. 131504(1–3).
[6] M. Feng, N. Holonyak Jr., H.W. Then, G. Walter, Charge control analysis of transistor laser operation, Appl. Phys. Lett. 91 (2007) pp. 053501(1–3).
[7] F. Dixon, et al., “Transistor laser with emission wavelength at 1544 nm”, Appl. Phys. Lett. 93 (15) (Jul. 2008) pp. 021111–1–021111-3.
[8] M. Feng, H.W. Then, N. Holonyak Jr., G. Walter, A. James, Resonance-free frequency response of a semiconductor laser, Appl. Phys. Lett. 95 (2009) pp. 033509(1–3).
[9] H.W. Then, M. Feng, N. Holonyak Jr., Microwave circuit model of the three-port transistor laser, J. Appl. Phys. 107 (2010) pp. 094509(1–7).
[10] Y. Huang, J.H. Ryou, R.D. Dupuis, F. Dixon, N. Feng, N. Holonyak Jr, “InP/ InAlGaAs light-emitting transistors and transistor lasers with a carbon-doped base layer,”, J. Appl. Phys. 109 (2011).
[11] Z. Duan, W. Shi, L. Chrostowsky, X. Huang, N. Zhou, G. Chai, Design and epitaxy of 1.5 µm InGaAsP-InP MQW material for a Transistor Laser, Optics Exp. 18 (2) (2010) 1501–1509.
[12] M. Shirao, T. Sato, Y. Takino, N. Sato, N. Nishiyama, S. Arai, Room-temperature continuous-wave operation of 1.3-µm transistor laser with AlGaInAs/InP quantum wells, Appl. Phys. Exp. 4 (7) (2011) pp. 072101-1–072101-3.
[13] M. Shirao, T. Sato, N. Sato, N. Nishiyama, S. Arai, Room temperature operation of npn-AlGaInAs/InP multiple quantum well transistor laser emitting at 1.3-μm wavelength, Opt. Exp. 20 (4) (2012) 3983–3989.
[14] Noriaki Sato, et al., Room-temperature continuous-wave operation of npn-AlGaInAs transistor laser emitting at1.3-μm wavelength, IEEE Photon. Tech. Lett. 25 (8) (2013) 728–730.
[15] B. Faraji, D.L. Pulfrey, L. Chrostowski, Small-signal modelling of the transistor laser including the quantum capture and escape lifetimes, Appl. Phys. Lett 93 (10) (2008) pp. 103509 (1-3).
[16] B. Faraji, W. Shi, D.L. Pulfrey, L. Chrostowski, Analytical modeling of the transistor laser, IEEE J. Sel. Top. Quantum Electron. 13 (2009) 594–603.
[17] L. Zhang, J.P. Leburton, Modeling of the transient characteristics of heterojunction bipolar transistor lasers, IEEE J. Quantum Electron. 45 (4) (2009) 359–366.
[18] M. Shirao, S. Lee, N. Nishiyama, S. Arai, “ Large signal analysis of a transistor laser“ *IEEE*, J. Quantum Electron. 47 (3) (2011) 359–367.
[19] I. Taghavi, H. Kaatuzian, J.P. Leburton, Bandwidth enhancement and optical performances of multiple quantum well transistor lasers, Appl. Phys. Lett. 100 (2012) pp. 231114 (1-5).
[20] R. Basu, B. Mukhopadhyay, P.K. Basu, “Estimated threshold base current and light power output of a transistor laser with InGaAs quantum well in GaAs base”, Semiconductor Sc. Tech. 26 (2011) pp. 105014(1–6).
[21] Rikmantra Basu, Bratati Mukhopadhyay, P.K. Basu, Analytical theory of a small signal modulation response of a transistor laser with dots-in-well in the base, Semicond. Sc. Technol. 27 (2012) pp. 015022(1–7).
[22] R. Basu, B. Mukhopadhyay, P.K. Basu, Modeling of current gain compression in common emitter mode of a transistor laser above threshold base current, J. Appl. Phys. 111 (2012) pp. 083103(1–7).
[23] R. Basu, B. Mukhopadhyay, P.K. Basu, Modeling resonance free modulation response in transistor lasers with single and multiple quantum wells in the base, IEEE Photon. J. 4 (5) (2012) 1572–1581.
[24] Rikmantra Basu, Bratati Mukhopadhyay, Prasanta K. Basu, Analytical model for threshold-base current of a transistor laser with multiple quantum wells in the base, IET-Optoelectron. 7 (3) (2013) 71–76.
[25] Pallab Bhattacharya, Jasprit Singh, Howard Yoon, Xiangkun Zhang, Augusto Gutierrez-Aitken, Yeeloy Lam, Tunneling injection lasers: a new class of lasers with reduced hot carrier effects, IEEE J. Quantum Electron. 32 (9) (1996) 1620–1629.
[26] M. Kucharczyk, M.S. Wartak, P. Weetman, P.-K. Lau, Theoretical modeling of multiple quantum well lasers with tunneling injection and tunneling transport between quantum wells, J. Appl. Phys. 86 (1999) 3218–3228.
[27] Neetesh Kumar, R. Basu, B. Mukhopadhyay, Tunnel injection transistor laser for optical interconnects, Opt. Quantum Electron. 50 (3) (2018) 1–12.
[28] V.V. Lysak, H. Kawaguchi, I.A. Sukhoivanov, Gain spectra and saturation power of asymmetric multiple quantum well semiconductor optical amplifiers, IEE Proc. Opto Electron. 152 (2) (2005) 131–139.